Chinese Chemical Letters 36 (2025) 110306

Contents lists available at ScienceDirect

Chinese Chemical Letters

journal homepage: www.elsevier.com/locate/cclet

Coordinating lithium polysulfides to inhibit intrinsic clustering behavior and facilitate sulfur redox conversion in lithium-sulfur batteries

Qihou Li [a], Jiamin Liu [a,*], Fulu Chu [a,c], Jinwei Zhou [a], Jieshuangyang Chen [a], Zengqiang Guan [a], Xiyun Yang [a], Jie Lei [b,*], Feixiang Wu [a,*]

[a] School of Metallurgy and Environment, National Engineering Research Centre of Advanced Energy Storage Materials, Central South University, Changsha 410083, China
[b] College of Materials Science and Engineering, Institute of New Energy Materials and Engineering, Fuzhou University, Fuzhou 350108, China
[c] School of Materials Science & Engineering, University of Jinan, Ji'nan 250022, China

ARTICLE INFO

Article history:
Received 2 June 2024
Revised 2 July 2024
Accepted 30 July 2024
Available online 31 July 2024

Keywords:
Lithium-sulfur (Li-S) battery
Polysulfide clustering
Coordinating reaction
Improved mediator
Shuttle effect

ABSTRACT

The intrinsic clustering behavior and kinetically sluggish conversion process of lithium polysulfides seriously limit the electrochemical reversibility of sulfur redox reactions in lithium-sulfur (Li-S) batteries. Here, we introduce molybdenum pentachloride ($MoCl_5$) into the electrolyte which could coordinate with lithium polysulfides and inhibit their intrinsic clustering behavior, subsequently serving as an improved mediator with the bi-functional catalytic effect for Li_2S deposition and activation. Moreover, the coordination bonding and accelerated conversion reaction can also greatly suppress the dissolution and shuttling of polysulfides. Consequently, such polysulfide complexes enable the Li-S coin cell to exhibit good long-term cycling stability with a capacity decay of 0.078% per cycle after 400 cycles at 2 C, and excellent rate performance with a discharge capacity of 589 mAh/g at 4 C. An area capacity of 3.94 mAh/cm^2 is also achieved with a high sulfur loading of 4.5 mg/cm^2 at 0.2 C. Even at -20 °C, the modified cell maintains standard discharge plateaus with low overpotential, delivering a high capacity of 741 mAh/g at 0.2 C after 80 cycles. The low-cost and convenient $MoCl_5$ additive opens a new avenue for the effective regulation of polysulfides and significant enhancement in sulfur redox conversion.

Lithium-sulfur (Li-S) batteries have been hailed as a promising alternative to conventional lithium-ion batteries owing to their high theoretical specific energy density (2600 Wh/kg), low cost, and environmental friendliness [1-5]. The sulfur redox reactions occurring in the Li-S battery positive electrode commonly involve the complicated multiphase transformation processes between elemental sulfur and the Li_2S discharge product accompanied by the generation of dissoluble lithium polysulfide intermediates (Li_2S_n, $4 \leq n \leq 8$) [6]. The dissolution and redeposition of polysulfide species are believed to enable the reversible conversion of the insulating sulfur/Li_2S particles *via* a solution-mediated reaction pathway [7-9]. However, some detrimental impacts are also caused. The dissolved polysulfide species would diffuse to the lithium metal anode and participate in the parasitic reactions during the cycling process, thus leading to the rapid capacity fading and poor cycling performance of Li-S batteries [10,11]. Most of the efforts to overcome this degradation mechanism have focused on trapping and/or confining the polysulfide species to reduce the active material loss by constructing functional sulfur hosts, modified separators or interlayers [12-18]. Furthermore, other issues of concern should include the intrinsic clustering behavior of lithium polysulfides and subsequently inadequate solution-mediated kinetics [9], which have often been overlooked by researchers.

Recent theoretical computation studies and molecular dynamics simulations demonstrate that the Li^+-S_n^{2-} bond network would be formed in the conventional ether-based electrolyte due to the electrostatic interactions between lithium cations and polysulfide dianions [19,20]. Lithium polysulfide monomers subsequently tend to aggregate to generate polysulfide clusters ($[Li_2S_n]_m$, $m > 1$), which are found to be the more stable configuration compared to discrete, isolated polysulfide chains, especially under low temperature [21,22]. Moreover, Anderson and colleagues presented that the major mechanism of Li^+ exchange is likely the dynamic processes involving the aggregation and dissolution of polysulfide clusters

* Corresponding authors.
E-mail addresses: liujiamin_2023@163.com (J. Liu), jielei@fzu.edu.cn (J. Lei), feixiang.wu@csu.edu.cn (F. Wu).

https://doi.org/10.1016/j.cclet.2024.110306
1001-8417/

that shuttle Li^+ from one cluster to another [23]. However, the dissociation into individual polysulfide chains and further lithiation would be greatly suppressed by the severe steric barriers and sturdy electrostatic connections in the highly tangled and disordered aggregates [24]. Moreover, the mass transport of polysulfide species would also be limited due to the large size of formed clusters, which could restrain the electrochemical reaction kinetics and following electrodeposition of Li_2S [8]. It is thus of utmost importance to develop efficient approaches to subdue the unfavorable polysulfide clustering behavior and facilitate the reaction kinetics of sulfur conversion.

Recently, the coordination configuration of lithium polysulfide clusters could be altered and disrupted through the introduction of additional ions and solvents in the electrolyte. For example, the coordination state of lithium salt and lithium polysulfide can influence and depend on each other due to the competitive electrostatic attraction between the salt anion and the polysulfide-adjoined lithium cation [25,26]. The addition of some strongly bonded lithium salts, such as lithium trifluoroacetate (LiTFA) and lithium nitrate ($LiNO_3$), can weaken the strong Li^+-S_n^{2-} bond network and mitigate the polysulfide clustering phenomena [27,28]. Similarly, the forcefully binding cationic groups, such as NH_4^+, also show the potential to deter the formation of undesirable clustered polysulfide aggregates because of the favorable NH_4^+-S_n^{2-} ionic associations [29]. In addition, solvents with high donor numbers, such as dimethylsulfoxide (DMSO) and dimethylacetamide (DMA), exhibit vigorous solvation with Li^+, which could contribute to the enhanced Li^+-solvent interactions and attenuated polysulfide clustering, thereby promoting the solution-mediated reactions of polysulfides [30,31]. Furthermore, the enhanced mediated effect also has been proposed in recent years by introducing a redox comediator to react with lithium polysulfides to afford the products with improved redox mediation capacity [32-36]. For example, diphenyl diselenide (DPDSe) is proven to spontaneously react with lithium polysulfides to generate lithium phenylseleno polysulfides (LiPhSePSs), which could reduce the energy barrier for multiphase sulfur conversion and increase the deposition dimension of Li_2S [34]. Moreover, the solubility and redox activity of polysulfide intermediates was effectively regulated by the functional couple molecules of 2,4-bis(*p*-tolythio)−1,3-dithia-2,4-diphosphetane-2,4-disulfide (BPHS) [37]. Sulfur conversion kinetics were consequently improved with the elimination of the shuttle effect, exhibiting excellent cycling performance of Li-S batteries.

Here, based on the principles of disrupting the Li^+-S_n^{2-} bond network of polysulfides and the improved mediation effect, we introduce molybdenum pentachloride ($MoCl_5$) into the electrolyte of Li-S batteries, which also has been reported as a dual-function redox mediator in Li-O_2 batteries [38]. Through a series of experimental and theoretical characterizations, $MoCl_5$ could voluntarily coordinate with lithium polysulfides *via* the formation of robust Mo-S bond. The as-produced complexes can not only inhibit the intrinsic clustering behavior of lithium polysulfides but also serve as an improved mediator with the bi-functional catalytic effect for Li_2S deposition and activation. Moreover, due to the coordination bonding and accelerated conversion reaction, the dissolution and shuttling of polysulfides also can be greatly restrained. When tested in a Li-S coin cell, this so-called polysulfide complexant allows for good long-term cycling stability with a capacity decay of 0.078% per cycle after 400 cycles at 2 C. Additionally, it demonstrates excellent rate performance with a discharge capacity of 589 mAh/g at 4 C. An area capacity of 3.94 mAh/cm^2 is achieved with a high sulfur loading of 4.5 mg/cm^2 at 0.2 C. The low-temperature performance is also evidenced at −20 °C, showing a high discharge capacity of 741 mAh/g after 80 cycles.

The commercially available $MoCl_5$ (Fig. S1 in Supporting information) was chosen and introduced into the electrolyte of the Li-S battery to explore its potential application for inhibiting intrinsic polysulfide clustering. As shown in Fig. 1a, the color of the Li_2S_6 solution would be changed from yellow to dark red after merging with the $MoCl_5$ solution. Moreover, the UV–vis spectrum of Li_2S_6 solution exhibits three significant absorption peaks at 630, 420, and 300 nm, corresponding to $S_3^{\bullet-}$, S_4^{2-}, and S_6^{2-} species, respectively [39]. After mixing with $MoCl_5$, the characteristic peaks of $S_3^{\bullet-}$ and S_4^{2-} would disappear, which should be attributed to the chemical interaction between polysulfides and $MoCl_5$. This also can be confirmed by Raman spectroscopy. As presented in Fig. 1b, the Li_2S_6 solution could demonstrate a characteristic Raman peak located at 450 cm^{-1}, assigning to the S_3^{2-}, S_4^{2-}, and S_4^- species [40], which are obviously observed to vanish after blending with $MoCl_5$. Furthermore, X-ray photoelectron spectroscopy (XPS) was conducted to clarify the specific interaction between $MoCl_5$ and Li_2S_6. As revealed in Fig. 1c, the XPS spectrum of S 2p for Li_2S_6 exhibits two typical terminal sulfur (S_T) and bridge sulfur (S_B) signals at 161.7/162.9 eV and 163.1/164.3 eV, respectively [41]. After reacting with $MoCl_5$, the additional peaks at the binding energy of 163.3/164.5 eV could be observed, belonging to the emergence of the Mo-S bonds accompanied by the weakened peak intensity of S_T. Moreover, in the XPS spectra of Mo 3d (Fig. S2 in Supporting information), the extra peaks at 232.5/235.7 eV could be monitored, validating the formation of Mo-S bonds. ^{7}Li NMR analysis was further conducted for the 0.1 mol/L Li_2S_4-containing electrolytes with or without $MoCl_5$ to investigate the effect of $MoCl_5$ on the polysulfides clustering. As shown in Fig. 1d, the ^{7}Li chemical shift moves upfield with the addition of $MoCl_5$, indicating the enhanced electron cloud density around Li^+, which should be induced by the construction of a stronger electron shielding environment due to the formed Mo-S bond [34,42]. All the above results evidentially demonstrate that $MoCl_5$ could spontaneously react with lithium polysulfides *via* the coordination between Mo and S_T, thus disturbing the intrinsic Li^+-S_n^{2-} bond network of polysulfides and alleviating the polysulfides clustering.

Symmetric cells were assembled based on Li_2S_6 electrolyte with or without $MoCl_5$ to evaluate the reaction kinetics of polysulfides conversion. As demonstrated in Fig. 1e, the polysulfides symmetric cell with $MoCl_5$ additive exhibits the higher current response, indicating that the coordination interaction of $MoCl_5$ can facilitate more adequate polysulfides conversion. Moreover, the corresponding electrochemical impedance spectra (EIS) display that the polysulfides symmetric cell with $MoCl_5$ additive shows a distinctly lower charge transfer resistance (R_{ct}, 902 Ω) compared with that in the absence of $MoCl_5$ (R_{ct}, 1451 Ω), further confirming the promoted polysulfides redox reactions (Fig. 1f). The spontaneous reaction trend has further been verified through theoretical calculations as the Gibbs free energy for the reaction of $MoCl_5$ and Li_2S_6 is −12.83 kcal/mol (Fig. 1g). Hence, their coordination reaction can proceed thermodynamically spontaneously to decouple the intrinsic clustering behavior of the intermediate polysulfides.

To further investigate the catalytic effect for Li_2S nucleation and activation, Li||Li_2S_8 cells were assembled to conduct the potentiostatic discharging and galvanostatic intermittent titration technique (GITT) tests, respectively. As displayed in Figs. 2a and b, and Fig. S3 (Supporting information), the Li||Li_2S_8 cell with $MoCl_5$ additive shows a Li_2S deposition capacity of 310.83 mAh/g, which is almost twice that of the blank cell (161.52 mAh/g). Besides, the cells were disassembled to characterize the deposited morphology of Li_2S *via* the SEM image. The insets demonstrate the typical lateral growth of Li_2S in the absence of $MoCl_5$, which would terminate the Li_2S nucleation after completely covering the conductive carbon substrate. By contrast, the smooth deposition and further two-dimensional growth of insulating Li_2S could emerge after the addition of $MoCl_5$, suggesting that the liquid-solid transformation from polysulfides towards Li_2S precipitation could be fa-

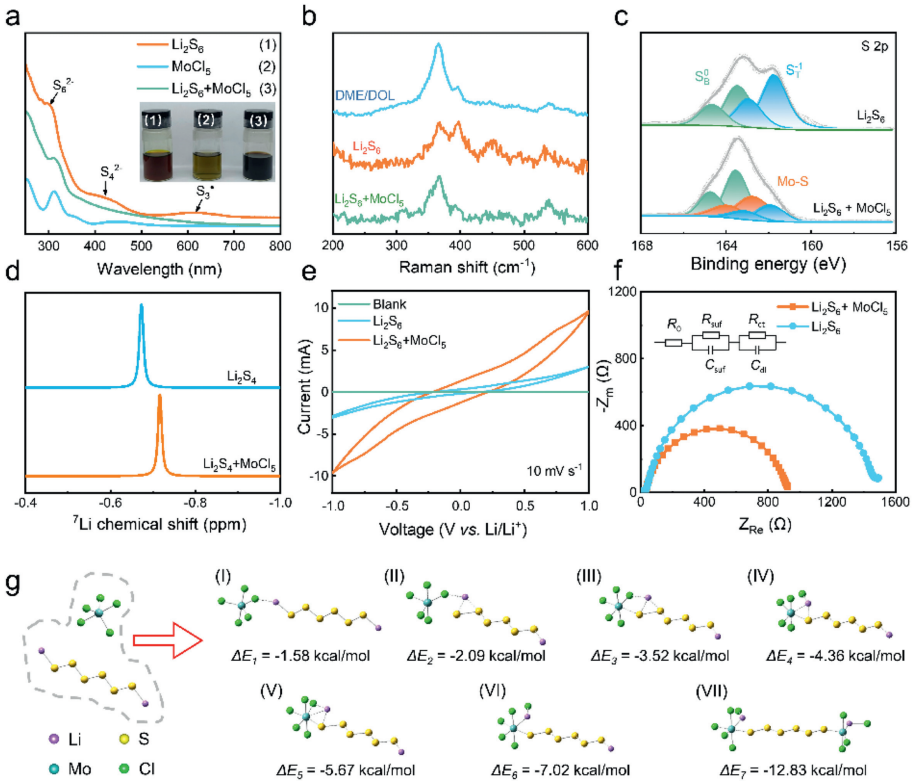

Fig. 1. Chemical interactions between $MoCl_5$ and lithium polysulfide. (a) The UV–vis spectra and corresponding optical photos of the supernatant (Li_2S_6, $MoCl_5$, and Li_2S_6+$MoCl_5$ solutions). (b) The Raman spectra of DME/DOL, Li_2S_6, and Li_2S_6+$MoCl_5$ solutions. (c) XPS spectra of S 2p for Li_2S_6 and Li_2S_6+$MoCl_5$. (d) ^7Li NMR spectra obtained from the DME/DOL-solvated Li_2S_4 with or without $MoCl_5$. (e) CV curves at a scan rate of 10 mV/s and (f) EIS spectra of Li_2S_6 and Li_2S_6+$MoCl_5$ symmetrical cells (the inset is the equivalent circuit diagram). (g) The Gibbs free energy for the reaction between Li_2S_6 and $MoCl_5$ from step I to step VII.

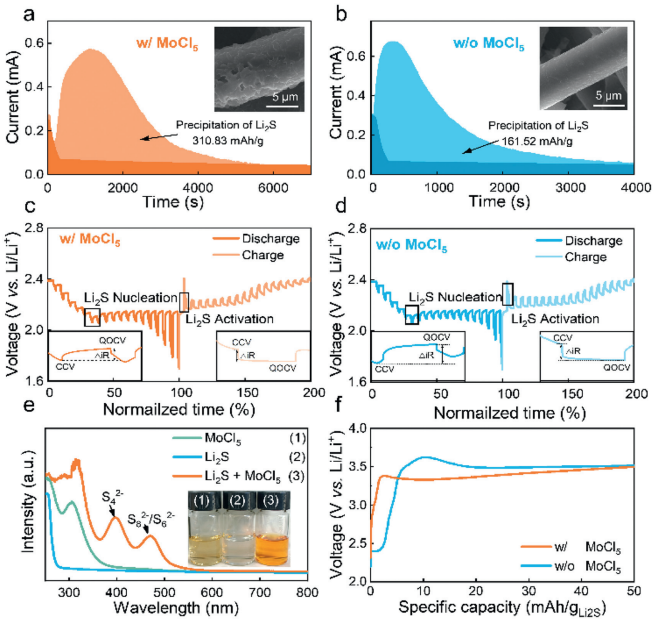

Fig. 2. Catalytic effect for Li_2S nucleation and activation. Potentiostatic discharge curves of Li_2S deposition (a) without and (b) with $MoCl_5$ and its corresponding SEM images. (c, d) GITT measurements. (e) The UV–vis spectra and corresponding optical photos of the supernatant ($MoCl_5$, Li_2S and Li_2S+$MoCl_5$ solutions). (f) Initial charging voltage profiles of Li||Li_2S cells with or without $MoCl_5$.

cilitated by coordinating with $MoCl_5$, then promoting the radial growth of Li_2S [42]. As presented in Figs. 2c and d, the internal resistance of each electrochemical reaction is proportional to the voltage difference between quasi-open-circuit-voltage (QOCV) and closed-circuit-voltage (CCV) at the same current [43]. The Li||Li_2S_8 cell with $MoCl_5$ additive shows visibly smaller internal resistance for Li_2S nucleation and activation than those without $MoCl_5$, which indicates that the introduction of $MoCl_5$ could alleviate polarization and kinetic limitations of Li_2S redox reactions [44].

Additionally, the interaction between Li_2S and $MoCl_5$ was studied. As shown in Fig. 2e, the colorless Li_2S solution turns aurantia after mixing with the $MoCl_5$ solution. The UV–vis absorption spectrum of the mixed solution is distinct from those of individual components. Two additional peaks could be observed at 480 nm and 400 nm, which should correspond to S_8^{2-}/S_6^{2-} and S_4^{2-} species, respectively [39]. This demonstrates that $MoCl_5$ can chemically oxidize Li_2S into polysulfides, thus showing the potential as the redox mediator to promote the activation of insulating Li_2S. Furthermore, Li_2S cathodes were prepared and utilized to assemble the Li||Li_2S cells. As illustrated in Fig. 2f, the activation energy barrier of Li_2S can be effectively reduced by adding $MoCl_5$ into the electrolyte, further confirming the mediation effect of $MoCl_5$ for Li_2S oxidation.

Optically transparent Li-S cells were fabricated with lithium metal anodes and sulfur cathodes with the sulfur content of 58.28 wt% (Fig. S4 in Supporting information). As shown in Fig. 3a, plenty of yellow species would be produced from the sulfur cathode and diffuse into the blank electrolyte during the cell discharging process at 0.1 C, which should be ascribed to the generation of soluble polysulfides. In comparison, the dissolution and shuttling of polysulfides can be visibly suppressed with $MoCl_5$ added into the electrolyte. In the discharge process of sulfur cathodes, the generated polysulfides would immediately coordinate with $MoCl_5$ to produce slightly soluble products (Fig. S5 in Supporting information), which achieves the same effect as reducing the solubility of polysulfides. Coupling with the inhibited polysulfides cluster-

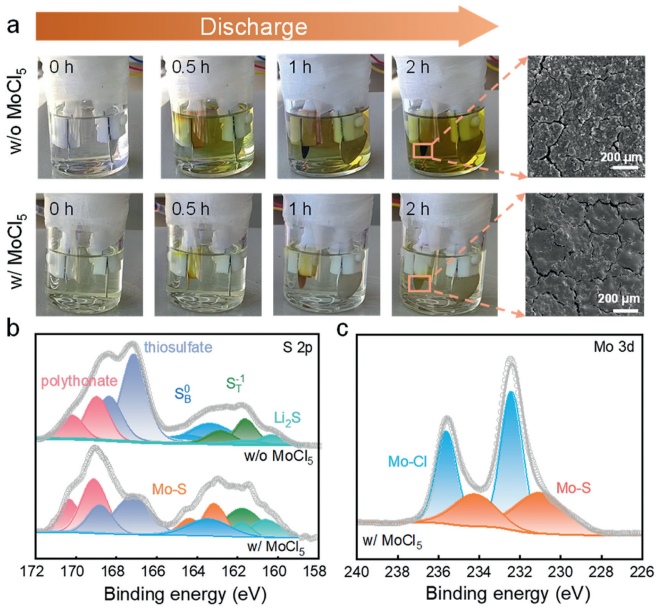

Fig. 3. Inhibition effect for polysulfides shuttling. (a) *In situ* visual observations of polysulfide dissolution and diffusion in glass beakers filled with the blank or $MoCl_5$-based electrolytes and the corresponding SEM images of sulfur cathodes in the fully discharged state; XPS spectra of (b) S 2p and (c) Mo 3d for sulfur cathodes collected from the beaker cells.

ing and faster reaction kinetics, the modified electrolyte can effectively suppress the polysulfides shuttle behaviors. Moreover, a yellow film-shaped layer is visually formed on the surface of the sulfur cathode, but this phenomenon is unobserved in the case of a blank electrolyte. The surface morphologies of the cathodes in the completely discharged state demonstrate that the sulfur electrode in the blank electrolyte would be rough and loose due to the dissolution loss of polysulfides, while a compact and smooth layer can be constructed to efficaciously inhibit the dissolution and diffusion of polysulfides. Furthermore, the chemical composition of the dense layer was characterized by XPS analysis. As displayed in the XPS spectra of S 2p in Fig. 3b, the peaks at 168.6/169.8 eV, 167.2/169.4 eV, and 160.6/161.8 eV correspond to typical polythionate, thiosulfate, and lithium sulfide (Li_2S) signals [41]. Compared to the sulfur cathode in the blank electrolyte, the peak intensity of thiosulfate is significantly reduced, and a new Mo-S peak appears after adding $MoCl_5$. Besides, the XPS spectra of Mo 3d also verify the formation of the Mo-S bond (Fig. 3c) [45]. It can be concluded that $MoCl_5$ reacts with polysulfides to form complexes *via* Mo-S bonds during the discharging process of sulfur cathodes, thereby effectively inhibiting the dissolution and diffusion of polysulfides.

To verify the catalytic behaviors of the sulfur redox reactions, cyclic voltammetry (CV) measurements were carried out. As shown in Fig. 4a, the first-cycle CV profiles of the Li-S coin cells exhibit two typical cathodic peaks at the potential of around 2.3 V and 2.0 V, attributing to the reduction of sulfur to soluble polysulfides, then to the insoluble Li_2S_2 and Li_2S. During the anodic segment, two corresponding oxidation peaks can be observed in the potential range of 2.3–2.5 V, which is ascribed to the oxidation of Li_2S_2/Li_2S to polysulfides and then back to elemental sulfur [46]. By introducing $MoCl_5$ into the blank electrolyte, the deposition and oxidation of Li_2S would exhibit higher redox peak current and lower polarization, which is consistent with the results in Fig. 2. The good repeatability of CV profiles in the subsequent cycles suggests the favorable reversibility of sulfur conversion (Fig. S6 in Supporting information). Accordingly, Li-S cells with different electrolytes were measured by CV at various scanning rates to evaluate the Li ions diffusion rates and reaction kinetics (Fig. S7 in Supporting information). Based on the Randles-Sevcik equation, a linear relationship between the peak current density and the square root of the scanning rate at each redox peak position suggests the typical characteristic of ion diffusion-controlled reactions [47]. The higher slopes for the Li-S cell using $MoCl_5$-based electrolyte reveal that the Li-ion transport between the formed $MoCl_5$-polysulfide complexes is more achievable [48]. EIS spectra of Li-S cells were conducted before and after 200 cycles at 1 C (Fig. 4b and Fig. S8 in Supporting information). When adding $MoCl_5$ to the electrolyte, the cell exhibits a lower charge transfer resistance (R_{ct}, 15.2 Ω) than the cell with blank electrolyte (31.6 Ω) before cycling. After 200 cycles, the R_{ct} (2.86 Ω) of the cell without $MoCl_5$ additive is still higher than the cell with $MoCl_5$ additive (1.84 Ω), indicating the accelerated charge transfer at the electrode surface in the presence of $MoCl_5$ [49]. Besides, as shown in Fig. S9 (Supporting information), the insulating discharging product of Li_2S exhibits a high potential barrier at the initial delithiation process in the cell with blank electrolyte at 0.2 C, while the addition of $MoCl_5$ significantly decreases the activation barrier [50].

As displayed in Fig. 4c, the Li-S cells with different electrolytes deliver subtle differences in discharge capacity at relatively low rates (0.1 C and 0.2 C), but the addition of $MoCl_5$ into electrolyte can enable the higher capacity contribution at high rates (≥0.5 C). Specifically, the cell with $MoCl_5$ additive could exhibit better rate performance, which provides the discharge capacity of 1261, 1136, 1002, 898, 810, 713, and 589 mAh/g at 0.1, 0.2, 0.5, 1, 2, 3 and 4 C, respectively (Fig. S10 in Supporting information). Besides, due to the strong interaction between $MoCl_5$ and polysulfides, the cell with $MoCl_5$ delivers higher capacity at the first plateau, which implies the increased sulfur utilization degree and rapid polysulfides conversion (Fig. S11a in Supporting information) [51]. The obvious valley between the first and second discharge plateaus represents the beginning of Li_2S nucleation. The cell with $MoCl_5$ additive displays a distinctly lower polarization voltage gap between Li_2S nucleation and activation at different rates (Fig. S11b in Supporting information), again confirming that the introduction of $MoCl_5$ can improve the electrochemical kinetics of the Li_2S redox reactions [43]. As shown in Fig. S11c (Supporting information), for the cell with $MoCl_5$, the increase of polarization voltage gap from 0.1 C to 4 C is only 256 mV (from 130 mV to 386 mV), which is considerably smaller than that of the cell without $MoCl_5$ (369 mV, from 124 mV to 493 mV).

The cycling performance of Li-S cells with different electrolytes was also tested at different rates. The optimal concentration of $MoCl_5$ additive is determined to be 5 mmol/L by comparative results (Fig. S12 in Supporting information), which has been used in other experiments unless otherwise stated. The cell employing a blank electrolyte presents an initial discharging capacity of 950 mAh/g, which would decrease continuously to 817 mAh/g after 150 cycles at 0.5 C (Fig. 4d). In contrast, after adding $MoCl_5$ into the electrolyte, the cell exhibits superior cycling performance with an initial discharge capacity of 1094 mAh/g and a retained capacity of 975 mAh/g for 150 cycles, which demonstrates a very competitive performance compared to the literature results (Table S1 in Supporting information). Even at a relatively higher rate of 2 C (Fig. 4e), the cell using $MoCl_5$ still delivers a discharge capacity of over 590 mAh/g after 400 cycles with a capacity-decay rate of 0.078% per cycle. As a comparison, the cell without $MoCl_5$ can only be cycled 238 times with a large capacity fade rate of 0.135%, which should be caused by the severe shuttle effect of polysulfides and the unfavorable growth of lithium dendrites. Furthermore, the cycling performance of the cell with $MoCl_5$ additive under high sulfur loading was evaluated. As shown in Fig. 4f, under high sulfur loading of 3.2, 3.5, and 4.5 mg/cm^2 and low E/S ratio (the ratio of electrolyte volume to sulfur mass) of 9, 8, and 6 μL/mg, the cells

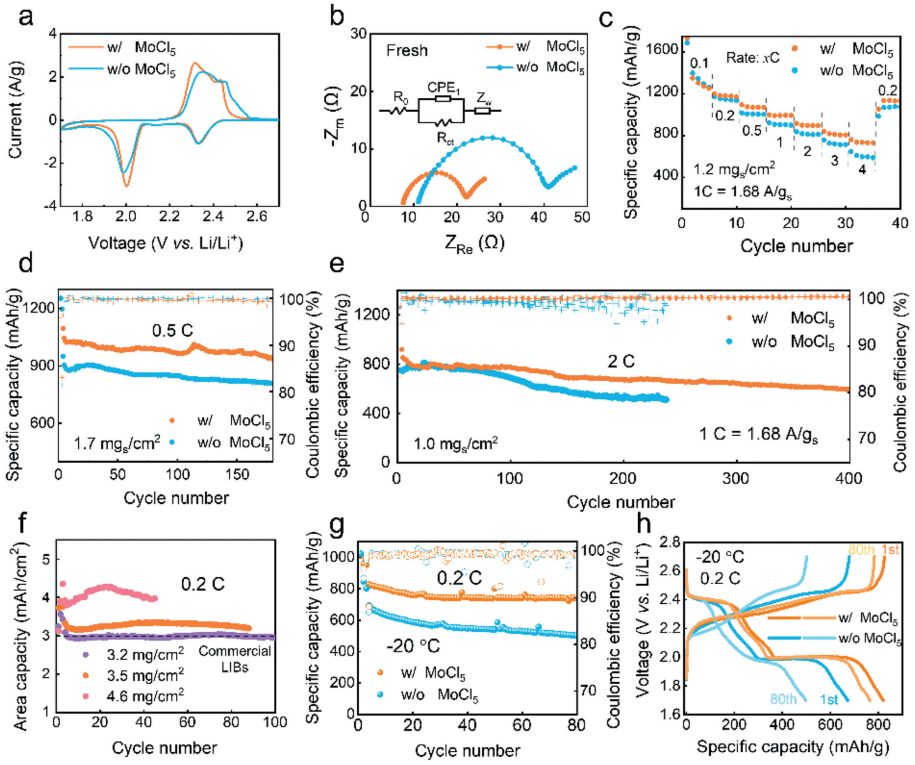

Fig. 4. Electrochemical performance of Li-S cells. (a) CV curves at the scan rate of 0.1 mV/s. (b) Nyquist plots of fresh Li-S cells. (c) Rate performance (sulfur loading: 1.2 mg/cm^2, 1 C corresponding to 1.68 A/g$_s$). (d) Cycling performance at 0.5 C (sulfur loading: 1.7 mg/cm^2). (e) Long-term cycling performance at 2 C (sulfur loading: 1.0 mg/cm^2). (f) Cycling performance of cells with $MoCl_5$ with high sulfur loading and electrolyte of 30 μL at 0.2 C. (g) Cycle performance and (h) corresponding charge/discharge curves at 0.2 C in −20 °C.

could exhibit outstanding initial specific capacities of 972, 949 and 902 mAh/g, which are corresponding to areal capacities of 3.1, 3.3 and 4.1 mAh/cm^2, respectively. Particularly, the cell with a sulfur loading of 3.5 mg/cm^2 can maintain good cycling stability with a capacity retention rate of 98% after 80 cycles. The two discharge plateaus at different cycles could be obviously observed (Fig. S13 in Supporting information), showing the satisfactory inhibition effect of $MoCl_5$ for polysulfides shuttling and the catalytic activity for sulfur conversion reactions.

Furthermore, the cycling performance of Li-S cells with or without $MoCl_5$ was estimated at low temperatures (−20 °C), where the polysulfides clustering issue has been believed to be more serious [52]. As shown in Fig. 4g, the cell using $MoCl_5$ can show good cycling stability at 0.2 C with a high discharge capacity of 741 mAh/g after 80 cycles. In comparison, the Li-S cell would be subjected to the obvious capacity fading with a discharge capacity of 504 mAh/g in the absence of $MoCl_5$. Moreover, the second discharge plateau corresponding to the Li_2S nucleation could still be maintained after cycling in the cell with $MoCl_5$, while that in the cell without $MoCl_5$ would almost vanish. The lower polarization voltage also further indicates the distinct catalytic effect and the suppressed behavior of polysulfides clustering (Fig. 4h).

In the end, the surface morphology of the sulfur cathodes and lithium metal anodes after battery cycling at a fully discharged state were characterized *via* SEM images. As shown in Fig. 5a, the cell with a blank electrolyte shows serious corrosion on the surface of the cycled Li anode after 200 cycles at 1 C. The morphology of the Li anode becomes rough, appearing irregular pores and dendrites. By adding $MoCl_5$ into the electrolyte, the relevant cycled Li anode shows high surface uniformity with large Li metal grains (Fig. 5b). This should be ascribed to the inhibiting effect of $MoCl_5$ for polysulfide shuttling, then limiting the erosion of metallic Li

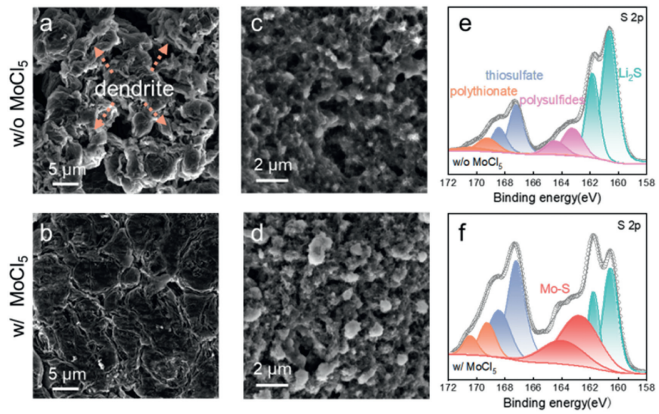

Fig. 5. Morphology and chemical characterizations of electrodes after battery cycling. The SEM images of (a, b) Li anodes and (c, d) sulfur cathodes. (e, f) XPS spectra of S 2p for sulfur cathodes from Li-S cells without or with $MoCl_5$ (after 200 cycles at 1 C) at a fully discharged state.

anodes by polysulfides. Furthermore, the microstructures of cycled sulfur cathodes are obviously diverse (Figs. 5c and d). Significantly fewer precipitations could be observed on the cycled sulfur cathode in the blank electrolyte, confirming the emergence of serious polysulfides shuttling. In the $MoCl_5$-based electrolyte, large particles would be formed and the interfacial passivation could be effectively prevented due to the three-dimensional pattern of nucleation and growth, which can promote sulfur utilization [53]. The interaction between $MoCl_5$ and the lithium metal anode is further clarified, and the introduction of $MoCl_5$ shows a great positive influence on the Li deposition morphology and cycling stability of the cells (Figs. S14 and S15 in Supporting information). Conse-

quently, Li-S cell with $MoCl_5$ demonstrates more standardized interface morphology and framework integrity of electrodes.

Besides, the interface composition of cycled electrodes also reveals the working mechanism of $MoCl_5$ *via* XPS analysis. Figs. 5e and f present XPS spectra of S 2p for cycled sulfur cathodes collected from cells with different electrolytes. Compared to the cathode with a blank electrolyte, the introduction of $MoCl_5$ induces new peaks of Mo-S bonds but without the polysulfides signal (162.8/164 eV) (Fig. S16 in Supporting information) [45,54]. This verifies that polysulfides could be effectively anchored *via* the Mo-S bond, helping to achieve the complete conversion of polysulfides to Li_2S. Moreover, other sulfur-containing species (polythionate and thiosulfate) with higher intensity can be clearly observed, which also has been proven to show mediation effect for polysulfides conversion [41]. Consequently, this inner mechanism can accelerate the reaction kinetics of sulfur conversion and thus increase the reversible capacity of the sulfur electrodes.

In summary, we introduce molybdenum pentachloride ($MoCl_5$) as an electrolyte additive to promote the electrochemical performance of Li-S batteries. The inorganic salt $MoCl_5$ could voluntarily coordinate with lithium polysulfides *via* the formation of tough Mo-S bonds to generate complexes, which can not only inhibit the intrinsic clustering behavior of lithium polysulfides, but also serve as a modified mediator with the bi-functional catalytic effect for Li_2S deposition and activation. In addition, the coordination bonding and accelerated conversion reaction can greatly restrain the dissolution and shuttling of polysulfides. Consequently, the Li-S coin cell with $MoCl_5$ electrolyte additive can exhibit good long-term cycling stability with a capacity decay of 0.078% per cycle after 400 cycles at 2 C, and excellent rate performance with a discharge capacity of 589 mAh/g at 4 C. An area capacity of 3.94 mAh/cm^2 is also achieved with a high sulfur loading of 4.5 mg/cm^2 at 0.2 C. Moreover, the modified cells work well at −20 °C with a high capacity of 741 mAh/g. In this work, we demonstrate the coordinated interaction of $MoCl_5$ with polysulfides and the optimized mediation effect, which could promote the efficient conversion of sulfur species and alleviate the capacity fading issue of Li-S batteries. Our work provides a new perspective for the rational design of electrolyte systems with multiple functions, including the polysulfide clustering inhibition and enhanced catalytic effect for high-performance Li-S batteries.

Declaration of competing interest

The authors declare that they have no known competing financial interests or personal relationships that could have appeared to influence the work reported in this paper.

CRediT authorship contribution statement

Qihou Li: Writing – original draft, Supervision, Methodology, Investigation, Formal analysis, Data curation. **Jiamin Liu:** Writing – original draft, Methodology, Investigation, Formal analysis, Data curation. **Fulu Chu:** Writing – original draft, Validation, Investigation, Formal analysis, Data curation. **Jinwei Zhou:** Validation, Methodology, Investigation. **Jieshuangyang Chen:** Validation, Methodology, Investigation. **Zengqiang Guan:** Validation, Methodology, Investigation. **Xiyun Yang:** Writing – original draft. **Jie Lei:** Writing – review & editing, Writing – original draft, Supervision, Methodology. **Feixiang Wu:** Writing – review & editing, Writing – original draft, Supervision, Resources, Project administration, Funding acquisition, Conceptualization.

Acknowledgments

The authors gratefully acknowledge the National Natural Science Foundation of China (Nos. 51904344, 52172264), and the Natural Science Foundation of Hunan Province of China (Nos. 2021JJ10060 and 2022GK2033).

Supplementary materials

Supplementary material associated with this article can be found, in the online version, at doi:10.1016/j.cclet.2024.110306.

References

[1] A. Manthiram, Y. Fu, Y.S. Su, Acc. Chem. Res. 46 (2012) 1125–1134.
[2] Y.X. Yin, S. Xin, Y.G. Guo, L.J. Wan, Angew. Chem. Int. Ed. 52 (2013) 13186–13200.
[3] F. Wu, F. Chu, G.A. Ferrero, et al., Nano Lett. 20 (2020) 5391–5399.
[4] R. Deng, M. Wang, H. Yu, et al., Energy Environ. Mater. 5 (2022) 777–799.
[5] R. Deng, F. Chu, F. Kwofie, et al., Angew. Chem. Int. Ed. 61 (2022) e202215866.
[6] Z. Wang, Y. Li, H. Ji, et al., Adv. Mater. 34 (2022) 2203699.
[7] G. Li, S. Wang, Y. Zhang, et al., Adv. Mater. 30 (2018) 1705590.
[8] J. Lei, T. Liu, J. Chen, et al., Chem 6 (2020) 2533–2557.
[9] Z. Guan, X. Chen, F. Chu, et al., Adv. Energy Mater. 13 (2023) 2302850.
[10] X. Fang, H. Peng, Small 11 (2015) 1488–1511.
[11] Y. Huang, L. Lin, C. Zhang, et al., Adv. Sci. 9 (2022) 2106004.
[12] X. Liu, J.Q. Huang, Q. Zhang, L. Mai, Adv. Mater. 29 (2017) 1601759.
[13] P. Wang, Z. Zhang, B. Hong, et al., J. Electroanal. Chem. 832 (2019) 475–479.
[14] J. Wu, T. Ye, Y. Wang, et al., ACS Nano 16 (2022) 15734–15759.
[15] D. Yang, J. Wang, C. Lou, et al., ACS Energy Lett. 9 (2024) 2083–2091.
[16] D. Yang, C. Li, M. Sharma, et al., Energy Storage Mater. 66 (2024) 103240.
[17] D. Yang, Y. Han, M. Li, et al., Adv. Funct. Mater. 34 (2024) 2401577.
[18] C. Li, D. Yang, J. Yu, et al., Adv. Energy Mater. 14 (2024) 2303551.
[19] R.S. Assary, L.A. Curtiss, J.S. Moore, J. Phys. Chem. C 118 (2014) 11545–11558.
[20] B. Wang, S.M. Alhassan, S.T. Pantelides, Phys. Rev. Appl. 2 (2014) 034004.
[21] C. Park, A. Ronneburg, S. Risse, et al., J. Phys. Chem. C 123 (2019) 10167–10177.
[22] A. Gupta, A. Bhargav, J.P. Jones, R.V. Bugga, A. Manthiram, Chem. Mater. 32 (2020) 2070–2077.
[23] A. Andersen, N.N. Rajput, K.S. Han, et al., Chem. Mater. 31 (2019) 2308–2319.
[24] M. Vijayakumar, N. Govind, E. Walter, et al., Phys. Chem. Chem. Phys. 16 (2014) 10923–10932.
[25] Q. Zou, Z. Liang, G.Y. Du, et al., J. Am. Chem. Soc. 140 (2018) 10740–10748.
[26] H. Chu, H. Noh, Y.J. Kim, et al., Nat. Commun. 10 (2019) 188.
[27] A. Gupta, A. Bhargav, A. Manthiram, ACS Energy Lett. 6 (2021) 224–231.
[28] S. Kim, J. Jung, I. Kim, et al., Energy Storage Mater. 59 (2023) 102763.
[29] A. Gupta, A. Bhargav, A. Manthiram, Chem. Mater. 33 (2021) 3457–3466.
[30] Q. Zou, Y.C. Lu, et al., J. Phys. Chem. Lett. 7 (2016) 1518–1525.
[31] A. Gupta, A. Bhargav, A. Manthiram, Adv. Energy Mater. 9 (2019) 1803096.
[32] Z. Lin, Z. Liu, W. Fu, N.J. Dudney, C. Liang, Adv. Funct. Mater. 23 (2013) 1064–1069.
[33] H.L. Wu, M. Shin, Y.M. Liu, K.A. See, A.A. Gewirth, Nano Energy 32 (2017) 50–58.
[34] M. Zhao, X. Chen, X.Y. Li, B.Q. Li, J.Q. Huang, Adv. Mater. 33 (2021) 2007298.
[35] H. Ye, J. Sun, X.F. Lim, Y. Zhao, J.Y. Lee, Energy Storage Mater. 38 (2021) 338–343.
[36] W. Zhang, F. Ma, Q. Wu, et al., Energy Environ. Mater. 6 (2023) e12369.
[37] Q. Zheng, Q. Hou, Z. Shu, et al., Angew. Chem. Int. Ed. 62 (2023) e202308726.
[38] X.G. Wang, Z. Zhang, Q. Zhang, et al., J. Mater. Chem. A 7 (2019) 14239–14243.
[39] J. Häcker, D.H. Nguyen, T. Rommel, et al., ACS Energy Lett. 7 (2022) 1–9.
[40] J.D. McBrayer, T.E. Beechem, B.R. Perdue, C.A. Apblett, F.H. Garzon, J. Electrochem. Soc. 165 (2018) A876.
[41] X. Liang, C. Hart, Q. Pang, et al., Nat. Commun. 6 (2015) 5682.
[42] H.J. Peng, G. Zhang, X. Chen, et al., Angew. Chem. Int. Ed. 55 (2016) 12990–12995.
[43] J. Park, E.T. Kim, C. Kim, et al., Adv. Energy Mater. 7 (2017) 1700074.
[44] Z. Wu, S. Chen, L. Wang, et al., Energy Storage Mater. 38 (2021) 381–388.
[45] H. Shi, Z. Sun, W. Lv, et al., J. Mater. Chem. A 7 (2019) 11298–11304.
[46] F. Liu, C. Zong, L. He, et al., Chem. Eng. J. 443 (2022) 136489.
[47] Y. Dong, D. Cai, T. Li, et al., ACS Nano 16 (2022) 6414–6425.
[48] K. Wu, Y. Hu, Z. Cheng, et al., J. Membrane Sci. 592 (2019) 117349.
[49] D.Q. Cai, J.L. Yang, T. Liu, S.X. Zhao, G. Cao, Nano Energy 89 (2021) 106452.
[50] H. Liu, P. Zeng, Y. Li, et al., J. Alloys Compd. 835 (2020) 155421.
[51] S. Chen, J. Luo, N. Li, et al., Energy Storage Mater. 30 (2020) 187–195.
[52] F. Chu, M. Wang, J. Liu, et al., Adv. Funct. Mater. 32 (2022) 2205393.
[53] H. Pan, J. Chen, R. Cao, et al., Nat. Energy 2 (2017) 813–820.
[54] M. Xiang, J. Li, S. Feng, et al., J. Colloid. Interface Sci. 624 (2022) 471–481.